Dynamic assembly of Hda and the sliding clamp in the regulation of replication licensing

Jin S. Kim[1], Michael T. Nanfara[2], Sundari Chodavarapu[3], Kyeong S. Jin[4], Vignesh M. P. Babu[2], Mohamed A. Ghazy[2], Scisung Chung[1], Jon M. Kaguni[3,*], Mark D. Sutton[2,*] and Yunje Cho[1,*]

[1]Department of Life Science, Pohang University of Science and Technology, 35398 Pohang, South Korea, [2]Department of Biochemistry, Jacobs School of Medicine and Biomedical Sciences, University at Buffalo, State University of New York, Buffalo, NY 14228, USA, [3]Department of Biochemistry and Molecular Biology, Michigan State University, East Lansing, Mi 48824-1319, USA and [4]Pohang Accelerator Laboratory, Pohang University of Science and Technology, 35398 Pohang, South Korea

ABSTRACT

Regulatory inactivation of DnaA (RIDA) is one of the major regulatory mechanisms of prokaryotic replication licensing. In RIDA, the Hda–sliding clamp complex loaded onto DNA directly interacts with adenosine triphosphate (ATP)-bound DnaA and stimulates the hydrolysis of ATP to inactivate DnaA. A prediction is that the activity of Hda is tightly controlled to ensure that replication initiation occurs only once per cell cycle. Here, we determined the crystal structure of the Hda–β clamp complex. This complex contains two pairs of Hda dimers sandwiched between two β clamp rings to form an octamer that is stabilized by three discrete interfaces. Two separate surfaces of Hda make contact with the β clamp, which is essential for Hda function in RIDA. The third interface between Hda monomers occludes the active site arginine finger, blocking its access to DnaA. Taken together, our structural and mutational analyses of the Hda–β clamp complex indicate that the interaction of the β clamp with Hda controls the ability of Hda to interact with DnaA. In the octameric Hda–β clamp complex, the inability of Hda to interact with DnaA is a novel mechanism that may regulate Hda function.

Regulation of DNA replication initiation is a critical event for maintenance of genomic stability and cell growth in all domains of life (1,2). To maintain genomic stability, DNA replication must be initiated once per cell cycle. Prokaryotic replication initiation starts by the assembly of a self-oligomer of ATP-DnaA at the chromosomal replication origin, *oriC*, followed by unwinding of the AT-rich DNA unwinding element within *oriC* (3,4). At the step of unwinding, ATP-DnaA is the active form. DnaA then recruits DnaB helicase that must be in a complex with its partner, DnaC, which inhibits the helicase and adenosine triphosphatase (ATPase) activity of DnaB (5). Activation of DnaB requires the dissociation of DnaC, which occurs by the interaction of primase with DnaB and concomitant primer synthesis (6). These primers are extended by DNA polymerase III (Pol III) holoenzyme, which is composed of three subassemblies: the core, the sliding clamp referred to in this report as the β clamp and the clamp loader (7). The β clamp is a ring-shaped homodimer that is loaded by the clamp loader onto the 3′-ends of primers to tether the core on DNA during DNA synthesis. Only the β clamp remains on the nascent DNA after Okazaki fragment synthesis; the core and the clamp loader are recycled (7).

Of the several independent mechanisms that inhibit reinitiation, one involves the hydrolysis of adenosine triphosphate (ATP) bound to DnaA by a DNA-bound complex of Hda and the β clamp. This process called the regulatory inactivation of DnaA (RIDA) may occur within the replisome or at *oriC* immediately following recruitment of the β clamp (1,8–11). In RIDA, Hda complexed with the β clamp and bound to double-stranded DNA directly interacts with DnaA to promote the hydrolysis of ATP bound to DnaA. The resultant ADP–DnaA is inactive in initiation (12–15). Thus, the cellular level of ATP-DnaA is highest prior to and at replication initiation, and then decreases during the elongation phase of DNA replication (13).

Regulation of Hda activity is also crucial to preserve cell viability (10,12). As evidence, Hda-deficient strains are very sensitive to variations in the cellular levels of DnaA because of lethal overinitiation. Likewise, overproduction of DnaA

---

*To whom correspondence should be addressed. Tel: +82 54 279 2288; Fax: +82 54 278 8111; Email: yunje@postech.ac.kr
Correspondence may also be addressed to Mark D. Sutton. Tel: +1 716 829 3581; Fax: +1 716 829 2661; Email: mdsutton@buffalo.edu
Correspondence may also be addressed to Jon M. Kaguni. Tel: +1 517 353 6721; Fax: +1 517 353 9334; Email: kaguni@msu.edu

causes overinitiation, which is toxic because of an increased steady-state level of double strand breaks that interfere with viability (16). In contrast, elevated Hda levels cause delayed replication initiation and induces the SOS response (17), or interferes with viability of a *dnaN159* strain, which expresses a mutant form of the β clamp (β159) that is apparently impaired in interacting with DNA polymerase III and translesion DNA polymerases (DNA polymerase II and IV) (18). Although the RIDA mechanism is best characterized in *Escherichia coli*, the fundamental notion represented by this pathway is that chromosomal duplication must be controlled so that it occurs only once per cell division cycle in all except meiotic cells (1). In addition to the role of Hda in RIDA, it is implicated in other biological roles of stabilization of DNA polymerase III at the replication fork and regulation of error-prone translesion DNA synthesis by DNA polymerase II and DNA polymerase IV (18).

Hda consists of an N-terminal domain that interacts with the hydrophobic cleft of the β sliding clamp via a conserved clamp-binding motif (QLSLF), and a C-terminal domain that contains sequence motifs of the AAA+ family of ATPases, and preferably interacts with atomic displacement parameters (ADP) (19,20). The arginine finger (Arg 153) in the conserved Box VII motif in the C-terminal domain is also essential for Hda function. In contrast to DnaA, which assembles as a multimer at *oriC*, Hda is active in RIDA as a monomer (20). Considering that the clamp-binding motif is hidden at the interface of a head-to-head homodimer in the crystal structure of *Shewanella amazonensis* (*Sa*) Hda bound to cytidine-diphosphate, the binding of ADP to Hda may facilitate dissociation of the dimer to the monomer (21). On the basis of these observations, dimerization of Hda may serve as a negative regulatory mechanism to control its function. Another model relies on the cellular abundance in *E. coli* of ∼50 monomers of Hda and ∼250–500 homodimers of the β clamp, which suggests that Hda exists solely as a complex with the β clamp (22). Hence, the physiological significance of Hda if it exists as a dimer and the role of ADP in stabilizing Hda as a monomer is unclear.

To understand how *E. coli* Hda interacts with the β clamp, we determined the crystal structure of this complex in which Hda is bound to ADP at 3.23 Å resolution. The structure reveals an unexpected hetero-octameric complex in which two Hda dimers are sandwiched between two β clamp rings. Of the two interacting surfaces, one interface is formed between the β clamp cleft and the conserved clamp-binding motif of Hda, which when altered inactivates Hda activity. Another critical interface is formed between the box VI and VII motifs of Hda and the middle domain of the β clamp. Disruption of this site inactivates Hda in RIDA. In the octameric complex, Hda dimerizes in a tail-to-tail manner, which blocks the active site arginine finger of each Hda protomer. This finding suggests that the octameric assembly negatively regulates Hda function. Based on the results of structural, biochemical and genetic analyses, we propose a novel mechanism of Hda regulation involving intermolecular interactions between Hda and the β clamp, as well as between Hda protomers.

MATERIALS AND METHODS

Cloning and purification of the Hda–β clamp complex

The genes encoding Hda or the β clamp were polymerase chain reaction (PCR)-amplified from *E. coli* genomic DNA and cloned into pET28a. The recombinant proteins were overproduced using *E. coli* BL21[DE3] grown at 37°C in LB media containing 50 μg/ml kanamycin, and induced by the addition of isopropyl β-D-1-thiogalactopyranoside to 0.4 mM at the culture OD_{600nm} of 0.8, followed by incubation at 37°C for 3 h. Following centrifugation, cell pellets were resuspended in Buffer A (20 mM Tris-HCl pH 7.4, 300 mM NaCl, 7 mM β-mercaptoethanol and 5% (v/v) glycerol). Cells that overproduced Hda or the β sliding clamp were mixed 1:1 (v/v), and lysed by sonication. The lysate was centrifuged in an SS-34 rotor at 18 000 rpm for 1h. The Hda–β clamp complex was purified by Ni-NTA affinity chromatography exploiting the His-tag at their N-termini. After elution from the column using Buffer A containing 300 mM imidazole, fractions containing the proteins of interest were diluted to 60 mM NaCl with Buffer B (20 mM Tris-HCl pH 7.4, 5 mM DTT and 5% (v/v) glycerol) and loaded onto a Resource Q column. Proteins were eluted using a linear gradient from 0 to 600 mM NaCl in Buffer B. Pooled fractions containing the Hda–β clamp complex were further purified by gel filtration chromatography (Superdex 200 16/60, GE Health Care Life Sciences) in Buffer C (20 mM Tris-HCl pH 7.4, 200 mM NaCl, 5 mM DTT and 5% (v/v) glycerol). Fractions containing the Hda–β clamp complex were pooled and concentrated by ultrafiltration to 30 mg/ml.

Crystallization and data collection

Crystals of the full-length Hda–β clamp complex were grown at 18°C by the hanging-drop vapor diffusion method. The crystallization buffer contained 0.1 M TrisHCl pH 7.0, 10.5% (w/v) PEG400, 0.2 M $CaCl_2$, 10 mM Trimethylamine-HCl, 1 mM ADP and 5 mM $MgCl_2$. Diffraction data were collected at −170°C using crystals flash-frozen in crystallization buffer containing 15%(v/v) glycerol. Diffraction data from native crystals were collected at 0.9786 Å on beamline 7A at the pohang advanced light source. Data integration, scaling, and merging were performed using the HKL2000 package (23, Supplementary Table S1).

Structure determination and refinement

The structure of Hda–β clamp complex was determined by the molecular replacement using PHENIX (24). The *Sa*Hda (PDBID: 3BOS) and *Ec* β clamp (2POL) structures were used as search models. The asymmetric unit contains four copies of Hda and four clamp molecules. After density modification (solvent flattening and non-crystallographic symmetry averaging), an electron density map generated at a resolution of 3.23 Å using the PHENIX program clearly revealed most of the regions for Hda and the β clamp. After building an initial model, successive rounds of model building using COOT (25) and refinement using PHENIX were performed. Refinements included interactive cycles of

rigid body refinement, bulk solvent corrections, positional and individual *B*-value refinement, TLS (translesion, libration and screw-motion) refinement and ADP refinement. A restrained non-crystallographic symmetry was applied throughout the refinement process. The final model consisted of Hda residues 4–226 (E and F chain), 5–180, 187–195 and 201–222 (G chain), 5–180, 190–194 and 199–209 (H chain). The model also contained residues 1–21 and 25–365 of the β clamp, and four ADP molecules. The final statistics are summarized in Supplementary Table S1.

Size exclusion chromatography (SEC)—multiangle laser light scattering (MALS) analyses

Size exclusion chromatography (SEC) experiments were performed using a Superdex 200 column (10/300 GL; GE Health Care Life Sciences), which was equilibrated with 20 mM Tris-HCl pH 7.4, 200 mM NaCl, 5 mM DTT and 5% (v/v) glycerol with DAWN EOS and OPTILAB DSP (Wyatt Technologies). Bovine serum albumin was used as an isotropic scatterer for detector normalization. The light scattered by a protein is directly proportional to its weight-average molecular mass and concentration. Wild-type or mutant (Hda^{W156A}-clamp, Hda^{hook}- β clamp or Hda- β$^{\Delta loop}$ clamp) Hda–β clamp complexes were injected onto the column. Except where noted, samples were prepared at a concentration of 2 mg/ml prior to SEC-MALS analysis. Sizes and oligomeric states of complexes were determined from the scattering curves using Astra V software (Wyatt Technologies). A lower concentration of wild-type Hda–β clamp complex (20 μg; 0.1 mg/ml) was also analyzed as described above but in buffer containing 150 mM NaCl.

Analytical ultracentrifugation

The molecular mass of the wild-type Hda–β clamp and Hda^{W156A}–β clamp complexes was analyzed by the sedimentation equilibrium technique with a Beckman Optima XL-A centrifuge. Sedimentation equilibrium data were evaluated using a nonlinear least-squares curve-fitting algorithm (XL-A data analysis software). All samples (wild-type Hda–β clamp at 19 μM, and Hda^{W156A}-β clamp at 10 μM) were analyzed in buffer containing 20 mM Tris-HCl pH 7.4, 200 mM NaCl, 5% β-mercaptoethanol and 5% (v/v) glycerol. For equilibrium analysis, absorbance scans at 280 nm at equilibrium at were collected at 12°C using a Beckman An60Ti rotor. The partial specific volume of the Hda–β clamp complex was estimated from the protein sequence to be 0.746 cm^3/g using the SEDNTERP program with a rho value of 1.021 for the molecular mass calculation.

Small angle X-ray scattering (SAXS)

Small angle X-ray scattering (SAXS) analyses of various concentrations of the Hda–β clamp complex (2, 3 and 4 mg/ml) were performed using the 4C SAXS II beamline of the Pohang Light Source II with 3 GeV power at Pohang University of Science and Technology (Korea). All sample solutions were prepared in Buffer C supplemented with 1 mM ADP. The light source from the in-vacuum undulator 20 (IVU 20: 1.4-m length, 20-mm period) of the Pohang

Light Source II storage ring was focused using a vertical focusing toroidal mirror coated with rhodium and monochromatized with an Si (111) double crystal monochromator, yielding an X-ray beam wavelength of 0.675 Å (18.360 KeV).

The X-ray beam size at the sample stage was 0.2 (V) X 0.6 (H) mm^2. A 2D charge-coupled detector (SX165, Mar USA, Inc.) was used with a sample-to-detector distance of 2.00 m. The magnitude of scattering vectors [q = $(4\pi/\lambda)$ sin θ; where 2θ is the scattering angle and λ is the wavelength of the X-ray beam source] was 0.10 nm^{-1} < q < 3.36 nm^{-1}. The scattering angle was calibrated with a polyethylene-*b*-polybutadiene-*b*-polystyrene block copolymer standard. Solution sample cells with 10-μm-thick mica windows, a volume of 50 μl and an X-ray beam path length of 0.8 mm were used. To monitor radiation damage, the SAXS data were collected in five successive frames of 0.1 min each. All scattering measurements were carried out at 4°C using an FP50-HL refrigerated circulator (JULABO).

Each 2D SAXS pattern was averaged circularly from the beam center and normalized to the X-ray beam intensity, which was monitored with a scintillation counter placed behind the sample. The scattering of the buffer solution was used as the experimental background. The theoretical SAXS curves were calculated from the crystal structures using the CRYSOL program [(26,27)].

Pull-down analysis

The full-length *dnaN* coding sequence was inserted into the plasmid pET28a-3XFLAG that was prepared by inserting 3X FLAG peptide sequences (derived from p3XFLAG-CMV-10) into pET28a. *E. coli* Rossetta (DE3) cells harboring plasmids encoding the β clamp joined to polyhistidine or the FLAG tag at the N-terminal end were grown in LB broth, induced with IPTG (0.4 mM) at OD$_{600nm}$ 0.5 and cultured overnight at 18°C. A total of 5 ml cell cultures were harvested and resuspended in 5 ml of lysis buffer (25 mM Tris-HCl pH 7.4, 200 mM NaCl, 7 mM 2-mercaptoethanol and 5% glycerol). Equal volumes (5 ml) of cells expressing the β clamp derivatives were combined with lysis buffer (final vol. 50 ml) in the absence or presence of excess purified Hda protein (0.4 mg) and lysed. After centrifugation at 18 000 rpm for 40 min, the supernatant was incubated with 0.1 ml Ni^{2+}-NTA beads (GE Healthcare) equilibrated in binding buffer (25 mM Tris-HCl pH 7.4, 200 mM NaCl, 7 mM 2-mercaptoethanol, 5% glycerol and 10 mM imidazole) for 1 h at 4°C. The beads were washed three times in 1 ml of binding buffer containing 50 mM imidazole and the recombinant proteins were eluted in 0.4 ml of binding buffer containing 250 mM imidazole. For pull-down analysis, samples eluted from the Ni^{2+}-NTA beads with or without Hda were diluted 6-fold in buffer (20 mM Tris-HCl pH 7.4, 100 mM NaCl, 7 mM 2-mercaptoethanol and 5% glycerol), then incubated with 0.2 ml Anti-Flag M2 agarose beads (Sigma) for 1 h at 4°C. The beads were washed three times with 1 ml of the buffer described above, and eluted with 0.4 ml of FLAG peptide (0.1 mg/ml) (Peptron) in this buffer. The eluates were analyzed by 15% sodium dodecyl sulphate-polyacrylamide gel electrophoresis (SDS-PAGE) stained with Coomassie Blue.

Construction of *E. coli hda* mutant strains

All *E. coli* strains used in this study were derived from MG1655. To cross the *hda* mutations onto the chromosome, we first made a strain bearing Δ*purC275*::*kan* Δ*diaA* Δ*hda*::(*cat-sacB*) alleles. The Δ*diaA* allele suppresses the defects associated with Δ*hda* (12, Babu *et al.*, in press). As the Δ*purC275::kan* allele is linked to *hda*, this drug resistance marker was used to move the *hda* alleles by P1vir transduction. The Δ*hda*::(*cat-sacB*) allele was constructed as follows: primers Hda-up-Bam-Fwd (gagggatccGGCGA TCACCCGTGTTTACAG) and Hda-up-BglII-Rev (caca gatctAGATACCTCAACCAGGATTTCAC) were used to PCR-amplify a 500 bp fragment corresponding to the promoter region upstream of the *hda* coding sequence; primers Cat-BglII-Fwd (cacagatctGAATAAATACCTG TGACGGAAGATC) and Cat-NheI-Rev (gaggctagcTAA ACCAGCAATAGACATAAGCGG) were used to amplify the 1 000 bp *cat* gene; primers SacB-NheI-Fwd (cacg ctagcGGAAAATAGAC CAGTTGCAATCC) and SacB-NotI-Rev (gaggcggccgcAACCGGATATCGGCATTTTC TTTTGCG) were used to PCR-amplify the 1 714 bp *sacB* allele; and primers Hda-down-NotI-Fwd (gaggcggccgcA TAAGGTGTTTATTGTCGGATGCG) and Hda-down-XhoI-Rev (cacctcgagACAATGACCAAACAGGTAAAA ATCTAC) were used to amplify a 500 bp fragment corresponding to the sequence immediately downstream from the *hda* coding sequence. These fragments were individually cloned into the Zero Blunt TOPO vector (ThermoFisher), then sequentially ligated at the unique BglII (Hda-up-Cat), NotI (sacB-HdaDown) or NheI (Hda-up-Cat-sacB-HdaDown) sites by standard ligation in Zero Blunt TOPO, ultimately generating plasmid pUCSD-PCR TOPO containing the Δ*hda*::(*cat-sacB*) locus flanked on either side by 500 bp of upstream or downstream *hda* sequences. To remove the chromosomal *hda* locus, the 3.7 kbp fragment was PCR-amplified from plasmid pUCSD-PCR TOPO using primers Hda-up-Bam-Fwd and Hda-down-XhoI-Rev, gel purified and electroporated into MG1655 bearing Δ*purC275*::*kan* Δ*diaA* as described previously (28). Replacement of the *hda*⁺ allele with the Δ*hda*::(*cat-sacB*) locus was confirmed by diagnostic PCR and nucleotide sequence analysis (Biopolymer Facility, Roswell Park Cancer Institute, Buffalo, NY, USA), as described previously (29,30). Using λ-Red recombineering, we replaced Δ*hda*::(*cat-sacB*) with each *hda* mutation. Recombinants were selected on LB agar supplemented with 10% (w/v) sucrose, and then confirmed to be Cam^S. Genomic DNA from randomly-selected Cam^S isolates was evaluated by DNA sequence analysis to verify the presence of the appropriate mutation (s). Once verified, we used P1vir to transduce the different *hda* alleles into isogenic derivatives of MG1655 by selection for the linked Δ*purC275::kan* allele. Transductants were verified by DNA sequence of PCR-amplified *hda*. We then replaced the Δ*purC275::kan* allele with *purC*⁺ using P1vir by selection of transductants on M9 minimal media lacking adenine, and again verified the presence of the appropriate *hda* allele by nucleotide sequence analysis.

Measure of hydroxyurea sensitivity

Cultures grown for 10 h were adjusted to similar cell densities based on OD_{600nm}, 10-fold serially diluted with sterile 0.8% saline and 5 μl aliquots of each strain were spotted onto LB agar plates containing the indicated concentrations of hydroxyurea (HU). After spotting, the plates were incubated overnight at 37°C prior to imaging.

Flow cytometry and quantitative PCR analysis of mutant *hda* strains

DNA content per cell was determined by flow cytometry essentially as described (31). Strains were subcultured 1:1 000 in LB media from overnight cultures and incubated at 37°C with shaking to an OD_{600nm} of 0.2. A portion of each culture was collected by centrifugation at 4°C, and resuspended in ice-cold TEG (Tris-EDTA-glycine) buffer containing 50 μg/ml RNase A, after which genomic DNA was extracted using phenol:chlorofo rm:isoamyl alcohol (pH 8.0), and backwashed with chloroform. Genomic DNA was precipitated at −80°C with sodium acetate and ethanol, resuspended in 50 mM Tris-HCl pH 8.0, 0.1 mM EDTA for use in quantitative PCR analysis (see below). The remaining portions of each culture were treated with 500 μg/ml rifampin and 25 μg/ml cephalexin to arrest protein synthesis and cell division, respectively. Cultures were incubated for an additional 2 h at 37°C with aeration. One milliliter of culture was fixed in 10 ml of 70% ethanol and stored at 4°C for >16 h. After centrifugation, the fixed cells were resuspended in 500 μl of phosphate-buffered saline (PBS; pH 7.4). The cells (0.1 ml) were then incubated with 20 μl of 1% PicoGreen dye (Invitrogen) in 25% DMSO for 1 h. Samples were analyzed using a Becton Dickinson FACSCalibur flow cytometer equipped with BD CellQuest™ v3.3 software and subsequently analysed with FCS Express v3.00.

Quantitative PCR was performed according to manufacturer's instructions (Bio-Rad). Briefly, PCR reactions contained 12.5 μl of 2 X iQ™ SYBR Green Supermix, 0.5 μl of (1:10 diluted) genomic DNA and 100 nM of *oriC*_1 5′-CTGTGAATGATCGGTGATCC-3′ primer paired with *oriC*_2 5′-AGCTCAAACGCATCTTCCAG-3′ primer, or with *TerC*_1 5′-CAGAGCGATATATCACAGC G-3′ primer paired with *TerC*_2 5′-TATCTTCCTGCTC AACGGTC-3′ primer in a 25 μl volume. PCR reactions were heated 95°C for 3 min, followed by 40 cycles with steps of 95, 56 and 72°C for 30 s each. The generation of specific PCR products was confirmed by melting curve analysis.

DNA replication assays

Wild-type β clamp, the $β^{Δloop}$ mutant clamp, wild-type Hda and the respective mutants were quantitated by the dye binding method (32) and also by SDS-PAGE after staining with Coomassie Blue. DNA replication assays were then performed to measure the activity of wild-type β clamp and the $β^{Δloop}$ mutant in experiments that measure the conversion of M13G*ori*1 ssDNA to the duplex form. Reaction conditions with this ssDNA (72 ng) contained SSB (4 pmol), primase (0.2 pmol), DNA polymerase III* (90 ng, 0.18 pmol), wild-type β clamp or the $β^{Δloop}$ mutant as indicated, dNTPs including ³H-TTP (0.1 mM each),

rNTPs (0.8 mM ATP; GTP, CTP and UTP each at 0.25 mM) in buffer containing 10 mM magnesium acetate and other components essentially as described (33,34). Incubation was for 10 min at 30°C. After quenching the reaction with trichloroacetic acid, the insoluble radioactive material was captured on glass fiber filters and radioactivity incorporated was measured by liquid scintillation spectrometry.

Alternatively, reactions contained a supercoiled *oriC*-containing plasmid, purified replication proteins and other required components (35). To determine the optimal level of the β clamp for RIDA assays, incubation was separated into two stages. The first incubation contained 40 mM HEPES-KOH pH 7.6, 20 mM Tris-HCl pH 7.5, 10 mM magnesium acetate, 4 mM DTT, 0.08 mg/ml bovine serum albumin, 4% (w/v) sucrose, 2 mM ATP, 0.5 mM each of CTP, GTP and UTP, 0.1 mM each of dATP, dCTP, dGTP and [methyl-^{3}H] dTTP (25–30 cpm/pmol), 40 mM phosphocreatine, creatine kinase (200 μg/ml), M13*oriC*2LB5 supercoiled DNA (200 ng; 46 fmol) and DNA polymerase III* (90 ng, 0.18 pmol) as the source of the clamp loader, β clamp or the β$^{\Delta loop}$ mutant as indicated and DnaA (110 ng; 2 pmol) in a volume of 23 μl. After the first incubation of 20 min at 30°C, a mixture (2 μl) that contained SSB (4 pmol), HU (0.3 pmol), DNA gyrase A subunit (3.8 pmol), DNA gyrase B subunit (5.8 pmol), DnaB (0.3 pmol as hexamer), DnaC (2 pmol) and primase (0.2 pmol) was added followed by incubation for 20 min at 30°C. DNA replication was measured as described above.

Assay of RIDA activity

To measure RIDA activity, two-stage replication assays were performed as described above. In one series of experiments, wild-type β clamp or the β$^{\Delta loop}$ mutant was added at 4.5 ng to reactions containing increasing amounts of wild-type Hda. In other experiments, increasing amounts of wild-type Hda or the respective mutants were added to reactions containing wild-type β clamp (56 ng). As above, acid-insoluble radioactivity retained on glass fiber filters was measured by liquid scintillation spectrometry.

ATP hydrolysis

Reactions to measure the influence of the β$^{\Delta loop}$ mutant in comparison with wild-type β clamp on the hydrolysis of radiolabeled ATP bound to DnaA were assembled essentially as described (35). Briefly, DnaA (2 pmol) was incubated in reactions containing 1.5 μM [γ^{32}P]-ATP for 15 min at 0°C. A mixture containing wild-type β clamp or the β$^{\Delta loop}$ mutant (56 ng), DNA polymerase III* (90 ng, 0.18 pmol), M13*oriC*2LB5 supercoiled DNA (200 ng, 46 fmol) and the indicated amounts of Hda were added to reactions containing 2 mM ATP and 30 μM ADP. Other experiments to compare the activity of the wild-type Hda with the respective mutants were performed as described above in reactions that contained a constant amount of β clamp (56 ng). After incubation for 20 min at 30°C, DnaA was then immunoprecipitated with Protein A agarose beads that were pre-incubated with rabbit antiserum that specifically recognize the DNA binding domain of DnaA, and the bound nucleotide was analyzed by polyethyleneimine-cellulose thin-layer chromatography.

RESULTS

Overall structure of the Hda–β clamp complex

We determined the structure of this *E. coli* Hda–β clamp complex at 3.23 Å resolution. The asymmetric unit contained four copies of Hda and two copies of the β clamp dimer (calculated molecular weight of 268 kDa, Figure 1A–D). In support, SEC-MALS analyses showed that the full-length *E. coli* Hda (26.6 kDa)–β clamp (40.6 kDa) complex eluted as a single peak with a molecular weight of 255 kDa (Figure 1A). As described in detail below, all four *Ec*Hda molecules contain an ADP and a magnesium ion at the nucleotide-binding site (Figure 1B–F). Like the ATPase domain of DnaA, the *Ec*Hda structure can be divided into a RecA-like base domain (residues 1–164) and a lid domain (165–233) (Figure 1E and Supplementary Figure S1A). The base domain consists of a five-stranded parallel β-sheet (in order of 2, 3, 4, 1 and 5) surrounded by nine helices; two helices (α1 and α2) are on one side and seven helices (α3–α9) are on the other. The lid domain formed by a four-helix bundle (α10–α13) is connected to the base domain via loop β5–α10. The sliding clamp assemble as a head-to-tail dimer in which 12 α-helices line the central cavity with a continuous layer of antiparallel β-sheet. Of its three domains (N-terminal (1–120), middle (121–248) and C-terminal (249–365) domains), Hda contacts the middle and C-terminal domains (Figure 1B).

The base domains of the four *Ec*Hda molecules are virtually identical with a r.m.s. deviation of 0.16–0.21 Å for 160 Cα atoms. By contrast, the lid domains are partly disordered in three Hda molecules (E, G and H protomer), which indicates that the lid domain of Hda is flexible. Those regions include residues of E (184–187, 219–221 and 232–233), G (181–186, 196–200, 219–221 and 228–233) and H (181–189, 195–199 and 209–233) (Supplementary Figure S1B). The β clamps of the Hda–β clamp complex are well aligned with the clamp-alone structure (chain A of each structure is aligned) with an r.m.s. deviation of about 1.2 Å. However, the dimeric interface of the clamps shows a distortion of 5° rotation and 8 Å translation along the z-axis compared with the structure of the β clamp alone, suggesting that complex formation with Hda leads to this altered structure (Supplementary Figure S1C).

The overall structure of the Hda–β clamp complex resembles an hourglass in which two dimers of Hda are sandwiched by the two β clamp rings. The dimensions of the octameric complex are $128 \times 118 \times 73$ Å^3 (Figure 1B and C). The channel through the two sliding clamp rings has a diameter of 37 Å that is large enough to accommodate duplex DNA (Figure 1D). In the side view, the Hda dimer is tilted by 20° relative to the y-axis (Figure 1C).

Hda interacts with the middle domain of the β clamp via its Box VI and VII motifs in its base domain (Figure 1F). Located in Hda's N-terminal region, each canonical clamp-binding motif [^{6}QLSLPL^{11}] of two Hda molecules interacts with each β clamp (Figure 1B–D and F). In addition, Hda interacts with a loop domain adjacent to the β clamp cleft (see below). To describe the organization of each Hda dimer, two protomers tightly associate with each other through the Hda homodimeric interface, which is primarily organized
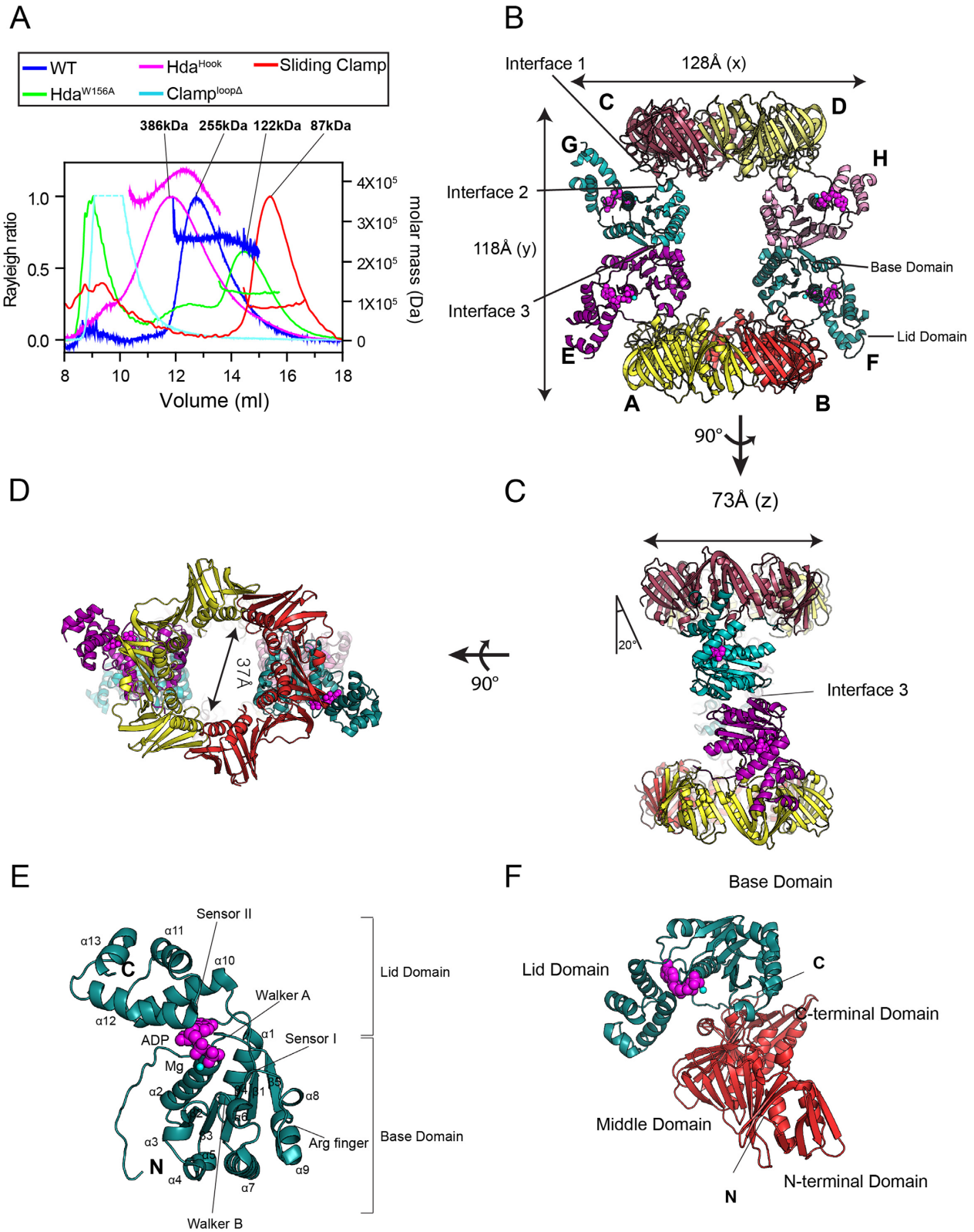
Figure 1. Structure of the Hda–β clamp complex. (**A**) SEC-MALS analysis of the Hda–β clamp complexes containing wild-type Hda or the indicated mutants, and of the β clamp alone. (**B**) Structure of the Hda–β clamp octameric complex in ribbon representation. Each β clamp is labeled A, B, C or D. Each Hda molecule is labeled E, F, G or H. ADP (magenta) and magnesium ion (cyan) in each Hda protomer are shown as spheres. Two orthogonal views of the Hda–β clamp complex structure in (**B**) are shown in (**C**) and (**D**). Interface 1, 2 and 3 are indicated in panels B and C. (**E**) Close-up view of the Hda molecule (chain F). The secondary structures, AAA+ conserved motifs and N- and C-termini of Hda are marked. (**F**) Heterodimeric arrangement of Hda (chain F) and the β clamp (chain B).

by the Box VI and VII motifs (Figures 1B–D and 2A). This interface is extensive and well organized with a buried surface area of about 1175 Å^2.

Key features of *Ec*Hda

As an AAA+ protein family member, *Ec*Hda harbors the Walker A (residues 50–57), Walker B (98–103), sensor I motif (Asp137) and the arginine finger (Arg153) in the base domain, and the sensor II (Arg202) motif in the lid domain (Figure 2A). These motifs play important roles in binding to nucleotide, metal ion and a water molecule in the nucleotide-binding site, and also in the hydrolysis of ATP bound to DnaA. Hda specifically binds ADP, which correlates well with the electron density consistent with ADP and not the other nucleotides at the junction between the base and lid domains (20, Figures 1E and 2B). The N-terminal loop, β1–α2 and β5–α10 loops, the α2 helix of the base domain and the α10 and α12 helices of the lid domain are also involved in ADP binding. In the nucleotide-binding site, the negative charges of the β phosphate of ADP are compensated by coordination of Gly55 (backbone), Arg56 and Ser57 that form the P-loop. In contrast, the α-phosphate of ADP does not interact with side chain residues (Figure 2B). The Mg^{2+} ion is bound by the α-, and β-phosphates of ADP and Ser57. A water molecule interacts with the β-phosphate, Mg^{2+} and Asn103. The adenine moiety of ADP is surrounded by the groove formed by the hydrophobic residues of the N-terminal loop and helices α10 and α12 of the lid domain (Figures 1E and 2B). Additionally, four hydrogen bonds with Trp23 (main chain), Glu17 and Arg177 stabilize the adenine base and ribose ring.

Located in the Box VII motif, the arginine finger (Arg153) of *Ec*Hda has a role in hydrolyzing ATP bound to DnaA (19, Figure 2A). In the crystal structure, the relative position of Arg153 is analogous to the arginine finger of *Sa*Hda (21). Whereas this residue in *Sa*Hda is fully exposed, the arginine finger in the *Ec*Hda–β clamp complex is buried by an opposing Hda molecule (Figure 2C). Hence, this form of the Hda–β clamp complex is presumably inactive because the arginine finger is unable to promote the hydrolysis of ATP bound to DnaA.

The *Ec*Hda–sliding clamp complex forms an octamer in solution

Several independent approaches support the conclusion that Hda and the β clamp form an octameric complex in solution. First, our SEC-MALS analyses determined a molecular weight of 255 kDa for the *Ec*Hda–β clamp complex (Figure 1A), which correlates with the calculated mass of 268 kDa of the octameric complex of four molecules of Hda and four β clamp protomers in the crystal structure.

Second, sedimentation equilibrium analysis by analytical ultracentrifugation of the *Ec*Hda–β clamp complex yielded a molecular mass of 260 kDa after global fitting to a single species model, using the data collected at rpm (Figure 3A). Third, SAXS analysis of the solution structure of the *Ec*Hda–β clamp complex revealed a radius of gyration (Rg) of 51.2 ± 2.24 Å, which is similar to that of the octameric crystal structure (Rg of 51.0 ± 0.045 Å, Figure 3B–D, Supplementary Tables S2 and 3). The observed light scattering

curve was comparable to the expected scattering curve calculated for the octameric crystal structure (Figure 3C). Superposition of the octameric crystal structure onto an averaged molecular envelope obtained from an *ab initio* SAXS shape reconstruction revealed close agreement (Figure 3D).

Fourth, pull-down experiments revealed the formation of an oligomeric *Ec*Hda–β clamp complex. The experimental design relied on derivatives of the β clamp that were affinity tagged with either hexahistidine or the Flag octapeptide. Cells induced to express either form of the β clamp were mixed under dilute conditions and then lysates prepared under low protein concentration in the absence or presence of purified Hda. The His-tagged β clamp was affinity purified with Ni^{2+}-NTA beads. After extensive washing, samples were incubated with anti-Flag beads and then analysed by SDS-PAGE. In the absence of Hda, the predominant polypeptide was the His-tagged β clamp, but a reduced level of the Flag-tagged β clamp was also observed (Figure 3E, lane 2 and 3). The presence of the latter may be explained by its non-specific binding to the Ni^{2+}-NTA beads, or by the formation of a heterodimer containing each form of the β clamp. In contrast with added Hda, a substantially greater amount of the Flag-derivative co-eluted with the His-tagged β clamp from the Ni^{2+}-resin or the Flag-resin (Figure 3E, lane 4 and 5). SEC analysis of the purified the Hda–β clamp complex (20 μg; 100 μg/ml) revealed that the size of the complex is about ∼300 kD (Figure 3F). On the basis of the evidence summarized here, we conclude that Hda and the β clamp form an octameric complex. These results contrast with size estimates ranging from 140–210 kDa in other studies (19,22).

Interaction between *E. coli* Hda and the β clamp

In the octameric complex, two interfaces (interface 1 and 2) are between Hda and the β clamp while the third (interface 3) is between Hda protomers (Figures 1B and 4A–D). In interface 1, Hda binds via its clamp-binding motif located in a flexible loop to the cleft between the middle and C-terminal domains of the β clamp (19,20, Supplementary Figure S1D). This interface is formed by interactions of Leu7, Leu9, Pro10 and Leu11 of Hda with the hydrophobic cleft of the sliding clamp containing the β10, β11 and β23 strands, the α8 helix, and the β14–α8, β21–β22 and C-terminal loops. Hydrogen bonds between Gln6 (Hda) and Met362 backbone (β clamp) and between Ser8 (Hda) and Gly174 backbone (β clamp) further stabilize interface 1 (Supplementary Figure S1D). Mutation of Gln6 or Leu9 of Hda to alanine significantly weakens complex formation between Hda and the β clamp, which demonstrates the importance of interface 1 (19). This interface is also conserved in the structure of the little finger domain (residues 243–351) of DNA polymerase IV complexed with the β clamp (36).

In interface 2, the hydrophobic patch of the strand-helix-helix (β2–α3–α4) motif of Hda is packed against loop α5–α6 and helix α6 of the middle domain of the clamp (Gln149, Val151, Tyr153 and Tyr154) (Figure 4B). Trp84 of Hda protrudes into the hydrophobic pocket composed of Pro196, Val237 and the aliphatic parts of several charged residues including Glu50, Asn156 and Lys235 of the β clamp.
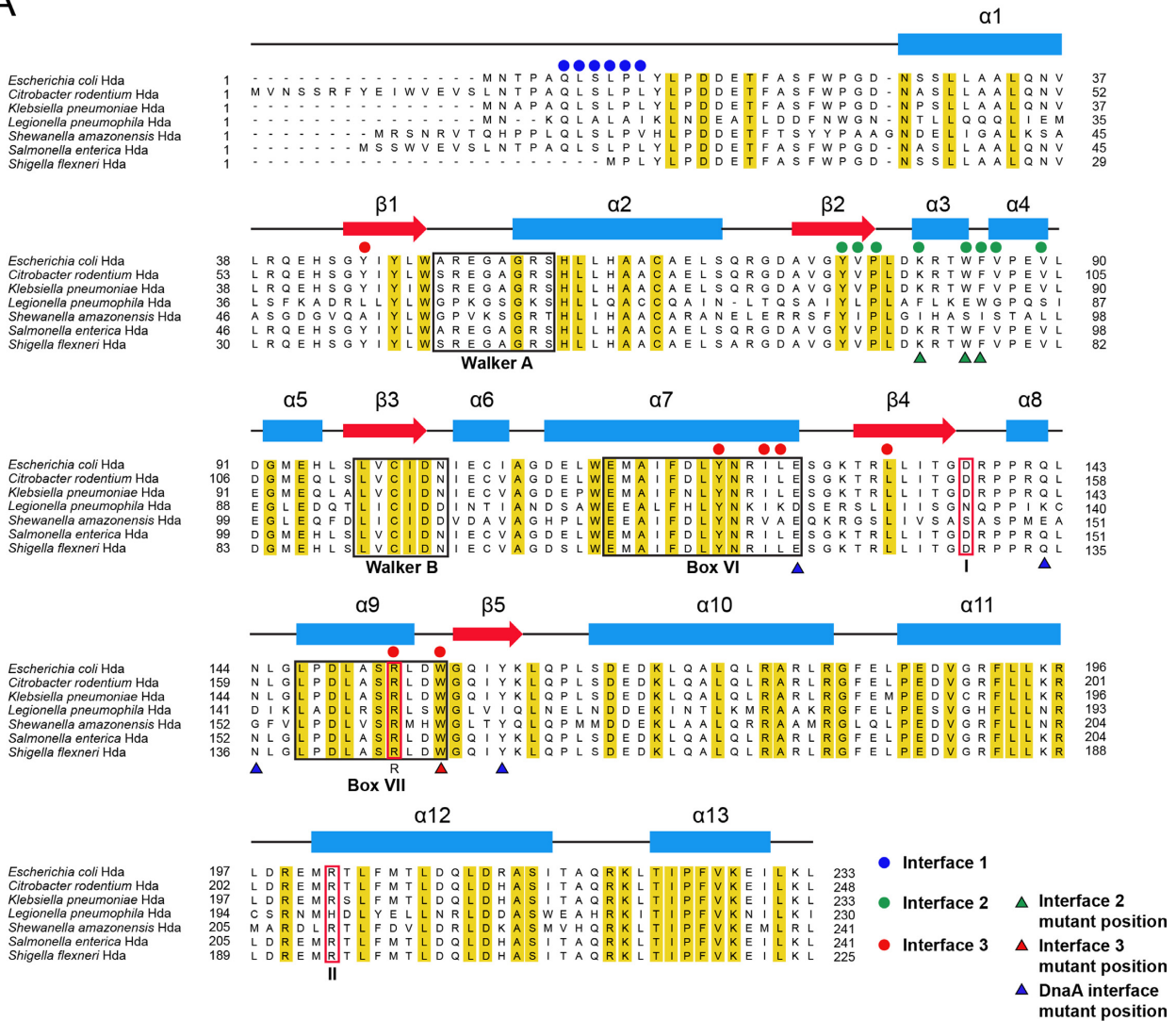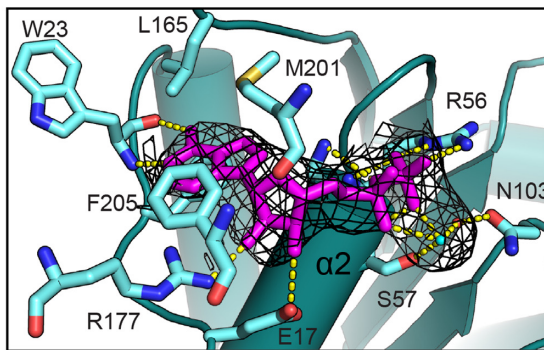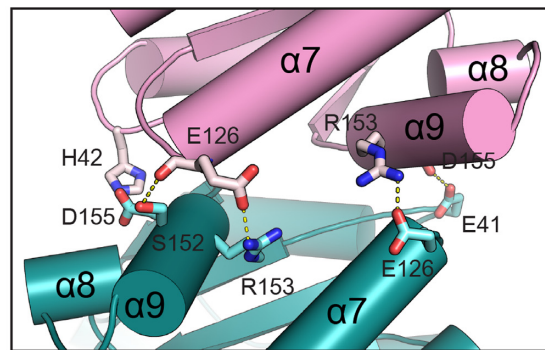
Figure 2. Secondary structure and key structural features of Hda (**A**) Sequence alignment of Hda from several bacterial species: *Escherichia coli, Citrobacter rodentium, Klebsiella pneumoniae, Legionella pneumophila, Shewanella amazonensis, Salmonella enterica* and *Shigella flexneri*. The secondary structural elements are shown at the top. The residues of interface 1, 2 and 3 are marked in blue, green or red dots, respectively. The substituted residues of the mutants used in SEC-MALS analyses are indicated by green and red triangles, and the residues mutated for DnaA binding are indicated by blue triangles. The conserved Walker A, Walker B, Box VI and Box VII motifs are denoted by black boxes. Sensor I, sensor II and arginine finger are shown in red boxes with I, II and R characters below, respectively. (**B**) The nucleotide-binding site of Hda (chain F). Residues surrounding ADP (magenta), Mg^{2+} ion (cyan dot) and a water molecule (red dot) are indicated. The electron density shown as a black mesh is a 2mFo-DFc simulated-annealing omit-map contoured at 1σ for ADP, Mg and the water molecule. Hydrogen bonds between ADP and surrounding residues are represented by yellow dots. (**C**) Close-up view of interface 3 that also shows the arginine finger in the E and G chains of Hda (purple and teal).
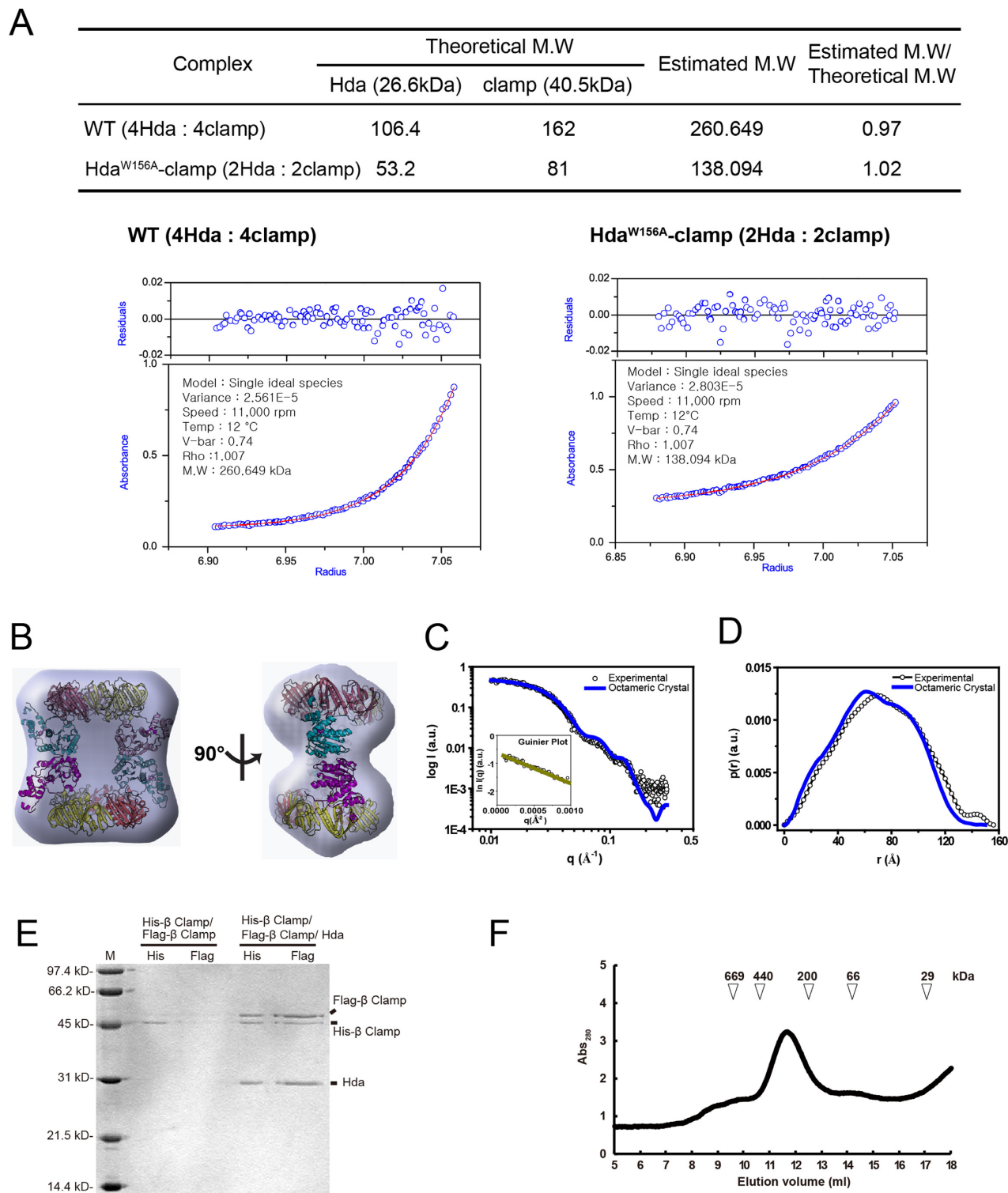
Figure 3. Analytical ultracentrifugation and SAXS analysis of the Hda–β clamp complex. (**A**) Sedimentation equilibrium data were evaluated using a nonlinear least-squares curve-fitting algorithm for the Hda–β clamp complex containing wild-type (WT) Hda or the W156A mutant. The expected sedimentation behavior for the Hda–β clamp complex is shown as a red line in comparison with the experimental data (blue circles). (**B**–**D**) SAXS analysis of the WT Hda–β clamp complex is shown. Blue envelopes are superimposed with the Hda–β clamp complex in two different orientations (**B**). The SAXS profile of the solution structure and the pair distance distribution functions [p(r)] for the Hda–β clamp complex are shown in (**C**) and (**D**). The experimental data are indicated by open circles, and the data calculated from the crystal structure are shown as solid blue lines. (**E**) Pull-down analyses of the His-β clamp and the Flag-β clamp in the absence or presence of Hda, as indicated. The lanes labeled 'His' contain the eluate from the Ni^{2+}-NTA bead pull-down. Likewise, lanes labeled 'Flag' contain samples from the subsequent anti-Flag pull-down of that same eluate. Positions of the Flag-β clamp, His-β clamp and Hda and molecular weight markers are indicated. (**F**) SEC profile of the Hda–β clamp complex at low concentration (100 μg/ml, 20 μg). The elution position of molecular weight markers are also shown.
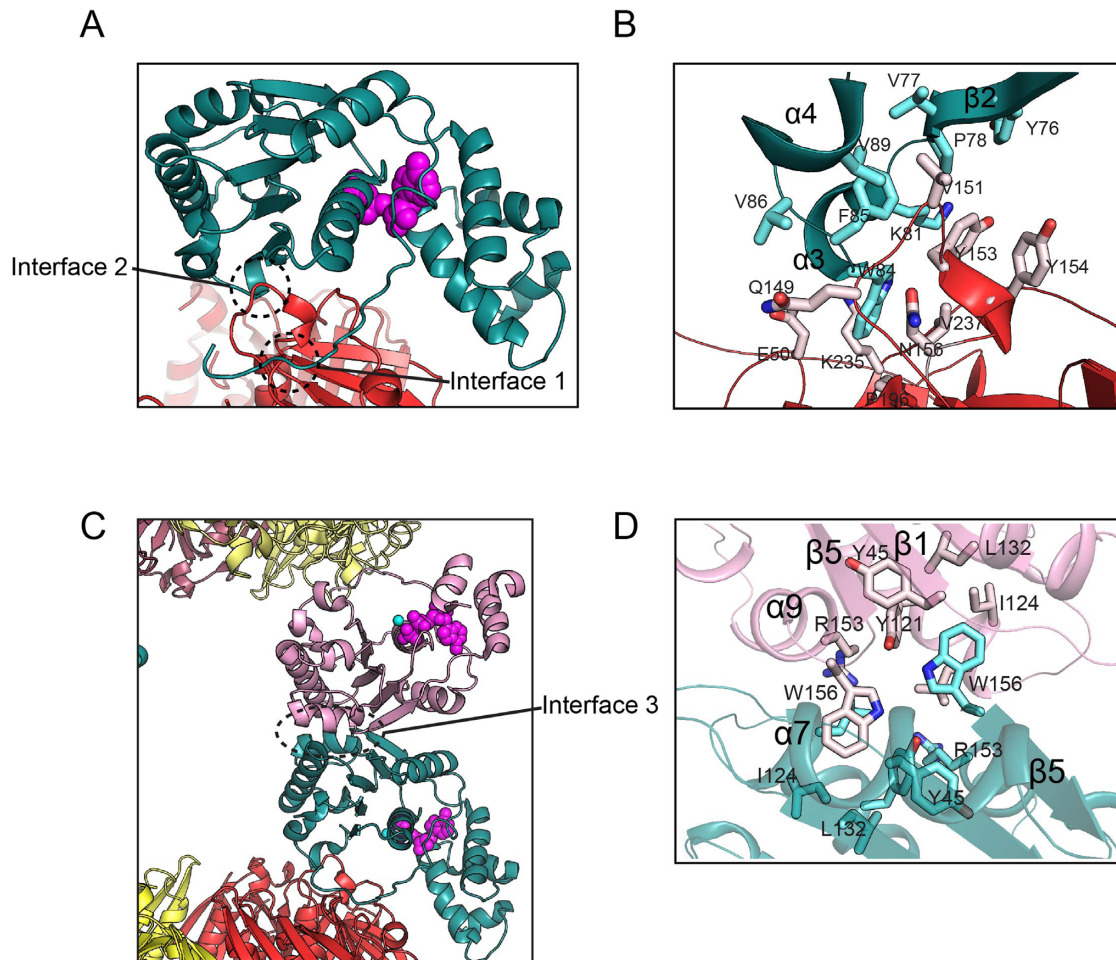
Figure 4. Three interfaces of the Hda–β clamp complex. (**A**) Interface 1 and 2 formed between Hda (Chain F; deep teal) and the β clamp (Chain B; red) are circled. (**B**) Close-up view of the interface 2. (**C**) Interface 3 is formed between the two Hda protomers. (**D**) Close-up view of the interface 3.

Verification of the Hda–β clamp interfaces

Residues of Hda that form interface 2 are relatively highly conserved among various bacterial species (Figure 2A). To understand the importance of interface 2 in complex formation between Hda and the β clamp, we constructed a mutant Hda bearing substitutions in the α3 helix (Hda^{hook}; K81S, W84S and F85S) (Figure 2A, green or red triangles). We also deleted residues from His148 to Tyr154 of the β clamp (β$^{\Delta loop}$). Unexpectedly, the Hda–β clamp complex assembled with the mutant Hda had a much greater molecular mass of 386 kDa compared with 255 kDa for the wild-type complex as measured by SEC-MALS analysis (Supplementary Table S4), suggesting that the Hda^{hook}–β clamp complex oligomerizes as a dodecamer. By comparison, the Hda–β$^{\Delta loop}$ clamp complex eluted near the void volume, suggesting that it is aggregated. It is unclear how the β$^{\Delta loop}$ mutation causes oligomerization of the complex. However, both mutant complexes appear to have a comparable ratio of Hda and the β clamp as the wild-type complex (Supplementary Figure S2). Apparently, the mutations trigger abnormal interactions at interface 2, leading to a higher oligomeric state of the Hda–β clamp complex. These observations underscore the importance of this interface in the assembly of the octameric complex.

Homodimeric interface between two Hda molecules

In the Hda–β clamp complex, interface 3 is symmetrically formed between two Hda protomers, and evidently stabilizes the octameric complex (Figure 4C and D). Helices α7 and α9 of two Hda molecules participate in the formation of interface 3, aligning Hda molecules in a tail-to-tail manner (Figures 2A and 4C). The hydrophobic pocket composed of Tyr45, Tyr121, Ilu124, Leu125, Leu132 and Arg153 of one protomer accommodates Trp156 in the α9 helix of the other Hda (Figure 4D). In SEC-MALS analysis, Hda bearing a W156A substitution and the β clamp form a tetramer rather than an octamer (Figure 1A and Supplementary Table S4), which indicates an important role for Trp156 in octamer formation. Other work showed that this residue is important for the hydrolysis of ATP bound to DnaA by Hda (13). Thus, although this mutant is able to form a tetramer, the W156A substitution significantly decreases the activity of Hda in RIDA (see below). Interface 3 is further stabilized by five hydrogen bonds between neighboring Hda pro-

tomers: E41 (F chain)-D155 (H chain), E126-R153, R153-E126, D155-H42 and S152-E126 (Figure 2C).

Interface 3 of the *Ec*Hda–β clamp complex is strikingly different from the interface of the *Sa*Hda dimer (Figures 2A and 5A; Supplementary Figure S3A). In the *Sa*Hda structure, two protomers form a head-to-head dimer through the secondary structural elements along the groove around the nucleotide-binding site. These elements include strands β1 (N-terminal loop; equivalent element in *Ec*Hda) and β3 (β2), and helices η1 (α3), η2 (α4), α3 (α7), α7 (α11) and α8 (α12) (21). Attempts to align the base domain of *Ec*Hda with that of *Sa*Hda (chains A and B) leads to collision around the dimeric interface that contains helices α3, α7 and α11, so an analogous structure cannot be formed (Supplementary Figure S3B and C).

Structural comparison of *Ec*Hda and *Sa*Hda

The secondary structures of *Sa*Hda are well conserved in *Ec*Hda (Figure 5B). As examples, the secondary structural arrangement around the nucleotide-binding site is highly similar between *Ec*Hda (15–166) and *Sa*Hda (22–174) with a r.m.s deviation of 1.5 Å. The lid domains of the two Hda molecules are aligned with a r.m.s deviation of 1.1 Å. Notably, the only small differences are the β1 strand of *Sa*Hda that is missing in *Ec*Hda and the α8 helix of *Ec*Hda that is absent in *Sa*Hda.

Regarding their tertiary structures, superpositioning by aligning the base domain reveals that the lid domain is rotated by 20° in *Ec*Hda compared with *Sa*Hda (Figure 5B). The α-phosphate of ADP protrudes out from the nucleotide-binding site of *Ec*Hda, whereas the corresponding phosphate of CDP in *Sa*Hda is in a different orientation (Figure 5C and D; Supplementary Figure S3D). Specifically, there is no interaction between the α-phosphate of ADP and the sensor II motif (Arg202) in *Ec*Hda, whereas the sensor II motif (Arg210) interacts with the α-phosphate of CDP and Glu24 (Glu17 of *Ec*Hda) in *Sa*Hda (Figure 5C and Supplementary Figure S3D). The lack of an interaction between sensor II and ADP results in rotation of the lid domain, which alters the arrangement of helices in the lid domain (Supplementary Figure S4A and B). The conformational difference of sensor II between *Ec*Hda and *Sa*Hda is reminiscent of the repositioning of the lid domain of *Aquifex aeolicus* DnaA, in which the change is attributed to the absence of an interaction of sensor II motif (Arg277) with the γ-phosphate of ATP that is lacking in ADP-bound *Aa*DnaA (37,38).

**In vivo analyses of Hda mutants**

The importance of the β clamp-binding motif of Hda and the cleft of the β clamp to form interface 1 is well established (19,39). To investigate the significance to RIDA function of interface 2 formed between Hda and the β clamp, interface 3 formed between Hda monomers, and the interface between Hda and DnaA, we mutated one or more residues within each of these surfaces and constructed MG1655 variants expressing these mutations from the native *hda* chromosomal locus. The following *hda* mutants were examined: the *Ec*Hda hook (K81S, W84S, F85S) targeting interface

2, and *Ec*Hda W156A (α9-β5) targeting interface 3 (Figure 2A). In addition, E126 (α7), Q142 (α8–α9), N144 (α8–α9) and Y160 (β5) residues of *Ec*Hda, which we predicted to interact with DnaA, were replaced with alanine (Figure 7B). Importantly, each of the mutant strains was viable, although the E126A mutant produced smaller colonies compared with the wild-type control, and one of the E126A clones acquired a second mutation at position K81 (K81R) in the hook region after passage that improved overall growth (Supplementary Figure S5). This and the poor growth phenotype of the E126A mutant suggest that it is impaired for RIDA.

To exclude the possibility that the poor growth phenotype of the E126A mutant is the result of poor expression, and to establish that the other mutants are expressed at comparable levels as wild-type Hda, immunoblotting experiments of whole cell lysates was performed. Although our anti-Hda polyclonal antibody was unable to detect the chromosomally-encoded level of Hda, it was able to detect an elevated level expressed from a low copy plasmid. Using this approach, we determined that each of the mutant Hda proteins was expressed at a level comparable to the wild-type control (Supplementary Figure S6). Thus, we conclude that the mutations failed to affect their steady-state levels appreciably, which may have been reduced if the substitutions alter the structure of Hda to make them susceptible to proteolytic degradation.

In addition to regulating initiation of DNA replication, RIDA also influences expression of *nrdAB*, which encode the *E. coli* class 1a ribonucleotide reductase (40). Because HU specifically scavenges the tyrosyl radical in NrdB, HU sensitivity serves as a measure of NrdB levels and thus RIDA (41,42,Babu *et al*., in press). The strain expressing *Ec*Hda bearing the E126A, E126-K81R, W156A or Y160A mutations showed significant sensitivity to HU, approaching the level of sensitivity observed for the RIDA-deficient Δ*hda* strain that also carries a Δ*diaA* mutation to suppress the growth defect of the Δ*hda* allele (12, Figure 6A). Importantly, the Δ*diaA* allele fails to alter the HU sensitivity of the Δ*hda* strain. In contrast, HU sensitivity of the Q142A and N144A mutants was comparable to the wild-type control, while the hook mutant (K81S, W84S, F85S) was modestly resistant at 8 mM HU, suggesting it might be more proficient than wild-type Hda at catalyzing RIDA. Both the modest HU resistance conferred by the hook mutant and the dramatic drop-off in viability at 8 mM HU was reproducible, suggesting this concentration of HU is saturating. Taken together, these results support the conclusion that E126 and Y160 contribute to Hda–DnaA interactions, which is required for RIDA, while disruption of interface 2 between Hda and the β clamp acts to stimulate RIDA, consistent with this contact serving to negatively regulate function of Hda in RIDA (Supplementary Table S5). Interestingly, the severe HU sensitivity of E126A is modestly relieved by the K81R mutant that resides at interface 2 (Figure 6A, ninth row). The W156A substitution was predicted to disrupt interface 3 between Hda monomers. However, previous analysis and the model shown below suggest that the surface containing Trp156 also interacts with DnaA for RIDA (15). Thus, it is possible that its increased level of HU
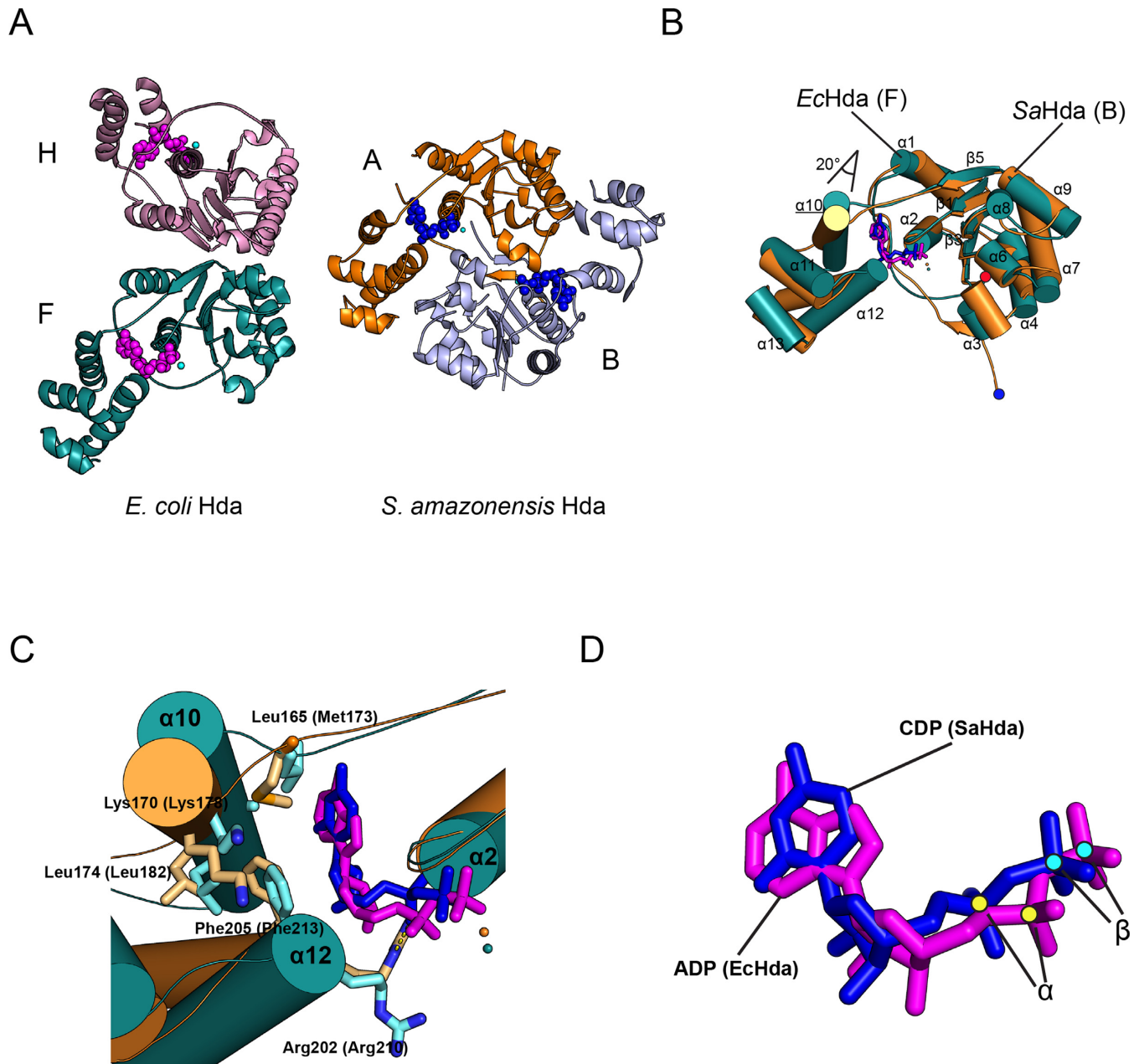
Figure 5. Comparison of the structures of the *Escherichia coli* Hda dimer with the *Shewanella amazonensis* Hda dimer. (**A**) The *E. coli* Hda dimer (chain F, teal; chain H, pink) in the Hda–β clamp complex is shown. Nucleotides are shown as pink spheres (left). The *S. amazonensis* Hda dimer (chain A, light blue; chain B, orange) is also shown. Nucleotides are shown in blue. The F chain of *Ec*Hda and the A chain of *Sa*Hda are displayed in the same orientation. (**B**) The superimposed structures of *Ec*Hda (chain F, teal) of the Hda–β clamp complex and *Sa*Hda (3BOS; chain A, orange) together with secondary structural elements are shown. ADP in *Ec*Hda and CDP in *Sa*Hda are shown in magenta and blue sticks, respectively. Each N-terminus of *Ec*Hda or *Sa*Hda is marked at the bottom with red or blue dots, respectively. (**C**) Close-up view of the nucleotide-binding site of the superimposed structures shows the interactions between nucleotide and hydrophobic residues of the lid domain. (**D**) The superimposed ADP and CDP of *Ec*Hda and *Sa*Hda, and the α-phosphate and β-phosphate marked by yellow or cyan dots are shown. The sticks are colored as in (**B**).

sensitivity reflects a defect in the interactions between Hda protomers, and/or between Hda and DnaA.

We also measured the cellular DNA content of the mutant *hda* strains using flow cytometry (Figure 6B). The wild-type strain showed major peaks at 2n and 4n positions, as did the *hda*-Q142A, *hda*-N144A and *hda*^{hook} mutants. In contrast, the *hda*-E126A, *hda*-E126A-K81R, *hda*-W156A and *hda*-Y160A mutants exhibited a single broad peak

greater than 4n (Figure 6B), indicating asynchronous initiation that is consistent with a RIDA defect. We also measured *oriC*:*TerC* ratios in these strains (Figure 6C). Compared with the wild-type control, the Δ*hda* Δ*diaA* strains displayed an expected significantly increased *oriC*:*TerC* ratio, indicating an excessive frequency of initiations. Whereas the *hda*-E126A mutant was also elevated, consistent with a RIDA defect, the other *hda* mutants included the *hda*-
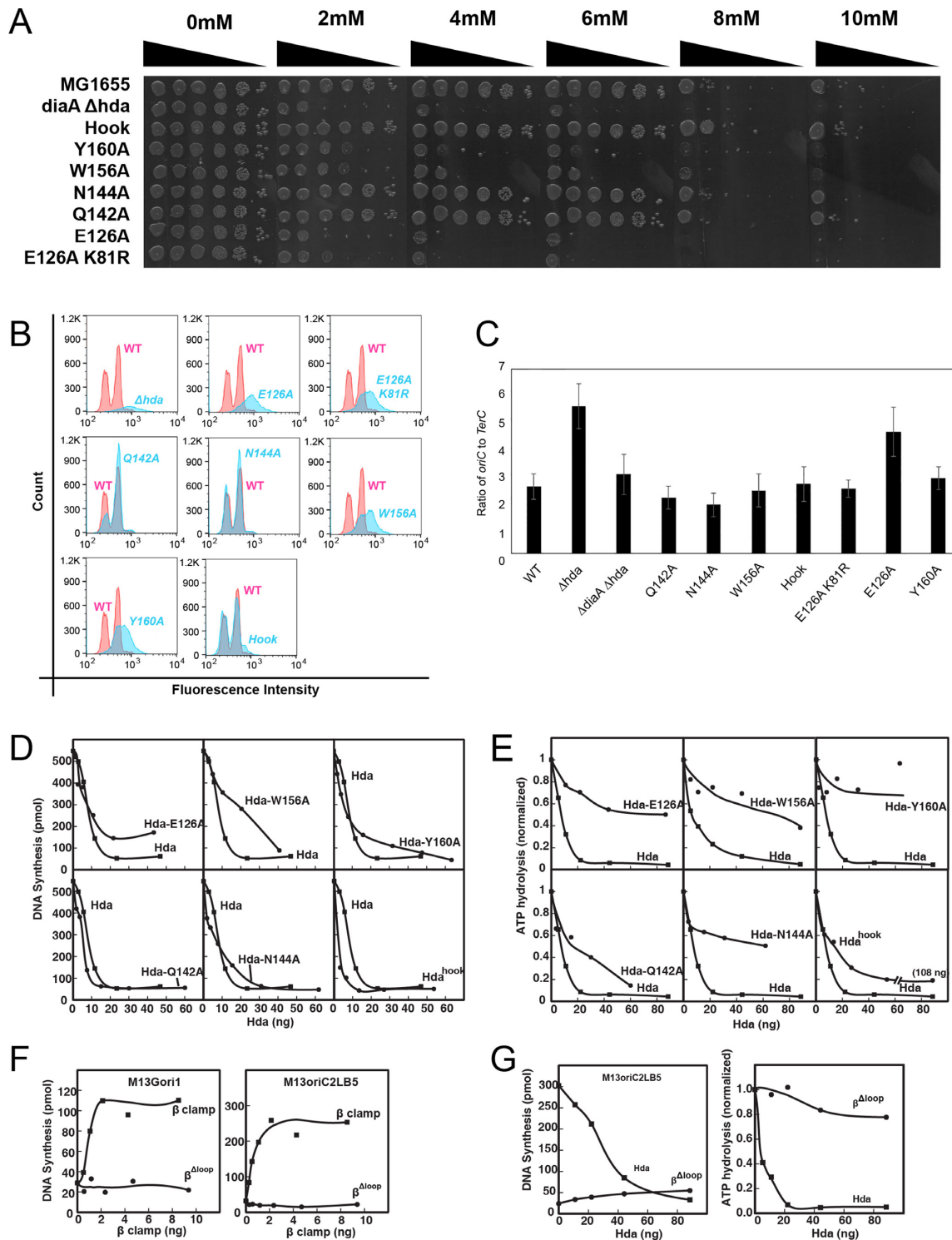
Figure 6. *In vivo* and *In vitro* analyses of Hda mutants (**A**) *In vivo* test of sensitivity of *Escherichia coli* mutants to hydroxyurea. After serial dilution, the sensitivity of *E. coli* strains encoding mutant Hdas to the indicated concentrations of HU was measured as described in 'Materials and Methods' section. Cultures were normalized for cell density based on OD_{600nm} prior to serial dilutions. (**B**) Flow cytometry analysis of strains expressing *hda* alleles. Cells (50 000) from the indicated strains were analyzed after staining with PicoGreen. Chromosome equivalents were determined using *E. coli* MG1655 as the control and shown in red in comparison with isogenic strains bearing the indicated *hda* allele shown in blue. Fluorescence intensity (abscissa) is presented in logarithmic scale. (**C**) Ratio of *oriC* to *TerC* of the strain encoding WT or mutant *hda*. (**D**) DNA synthesis was measured in reactions containing a supercoiled plasmid bearing *oriC* in the presence of WT Hda or mutants as described in 'Materials and Methods' section. (**E**) Hydrolysis of ATP bound to DnaA by WT Hda or mutants. (**F**) DNA synthesis was measured in reactions containing M13G*ori*1 ssDNA (left) or M13*ori*C2LB5 supercoiled DNA (right), other reaction components and increasing amounts of WT β or the $β^{\Delta loop}$ clamp mutant followed by incubation at 30°C for 10 or 20 min as described in 'Materials and Methods' section. (**G**) Influence of the $β^{\Delta loop}$ clamp mutant on the activity of DnaA in the RIDA assay that measures DNA replication of an *oriC*-containing plasmid (left) and ATP hydrolysis (right).

E126A-K81R were similar to the wild-type strain, suggesting that their RIDA defect was not as severe as the *hda*-E126A mutant.

The Hda mutants are defective in RIDA activity *in vitro*

Using an *in vitro* assay reconstituted with purified components (35), we measured the level of inhibition caused by the mutant Hda proteins on the DnaA-dependent DNA replication of a supercoiled DNA carrying *oriC*. Considering that Hda forms a complex with the β clamp, which was present at 0.7 pmol per reaction, we presume that the negligible inhibition at lower levels is due to the insufficient amount of Hda complexed with β clamp (Figure 6D). However, intermediate levels of E126A, W156A and Y160A were only partially inhibitory compared with the greater inhibition observed with other mutants and wild-type Hda. In the assay that measures the hydrolysis of ATP bound to DnaA (Figure 6E), the E126A, W156A and Y160A mutants were defective, which suggests that their lesser ability to stimulate ATP hydrolysis leads to both increase sensitivity to HU, and less frequent initiation as measured by flow cytometry (Figure 6A and B). In comparison, the hook mutant was only slightly less active than wild-type Hda, which conforms with an initiation frequency of the corresponding mutant that is comparable to a wild-type *hda* strain (Figure 6C). Apparently, the substitutions in Interface 2 of the hook mutant do not substantially impair the ability of Hda to interact with the β clamp or possibly DnaA. The conundrum is that this mutant's HU resistant phenotype (Figure 6A) suggests that the mutant is hyperactive for RIDA *in vivo*.

As described in the Introduction, an increased proportion of ATP–DnaA to ADP–DnaA is thought to lead to initiation (4). Correspondingly, a decreased ratio of ATP–DnaA to ADP–DnaA has the opposite effect. Considering that Q142A exhibited a similar inhibitory effect as wild-type Hda in Figure 6D and in the genetic assay of Supplementary Table S3, these results suggest that despite the reduced ability to stimulate the hydrolysis of ATP bound to DnaA compared with wild-type Hda, this level of activity causes inhibition of initiation in vitro (Figure 6D and E).

The $\beta^{\Delta\text{loop}}$ clamp mutant is defective in DNA replication in RIDA, and in stimulating the hydrolysis of ATP bound to DnaA

The $\beta^{\Delta\text{loop}}$ mutant lacks essential residues at interface 2 that interact with DNA during loading of the β clamp (30,43). Hence, this mutant is predicted to be inactive in DNA replication and in RIDA. To validate the results of the other mutants described in this study, the $\beta^{\Delta\text{loop}}$ mutant was analyzed as a control in several in vitro assays. In two independent DNA replication assays (30,43), the $\beta^{\Delta\text{loop}}$ clamp mutant was found to be inactive in comparison with the wild-type β clamp (Figure 6F). These results are consistent with a defect of the mutant in DNA binding required for clamp loading.

The $\beta^{\Delta\text{loop}}$ clamp mutant was also examined for its influence on the activity of DnaA under reaction conditions comparable to Figure 6D. Compared with the level of inhibition observed with wild-type β clamp, the $\beta^{\Delta\text{loop}}$ mutant was inactive (Figure 6G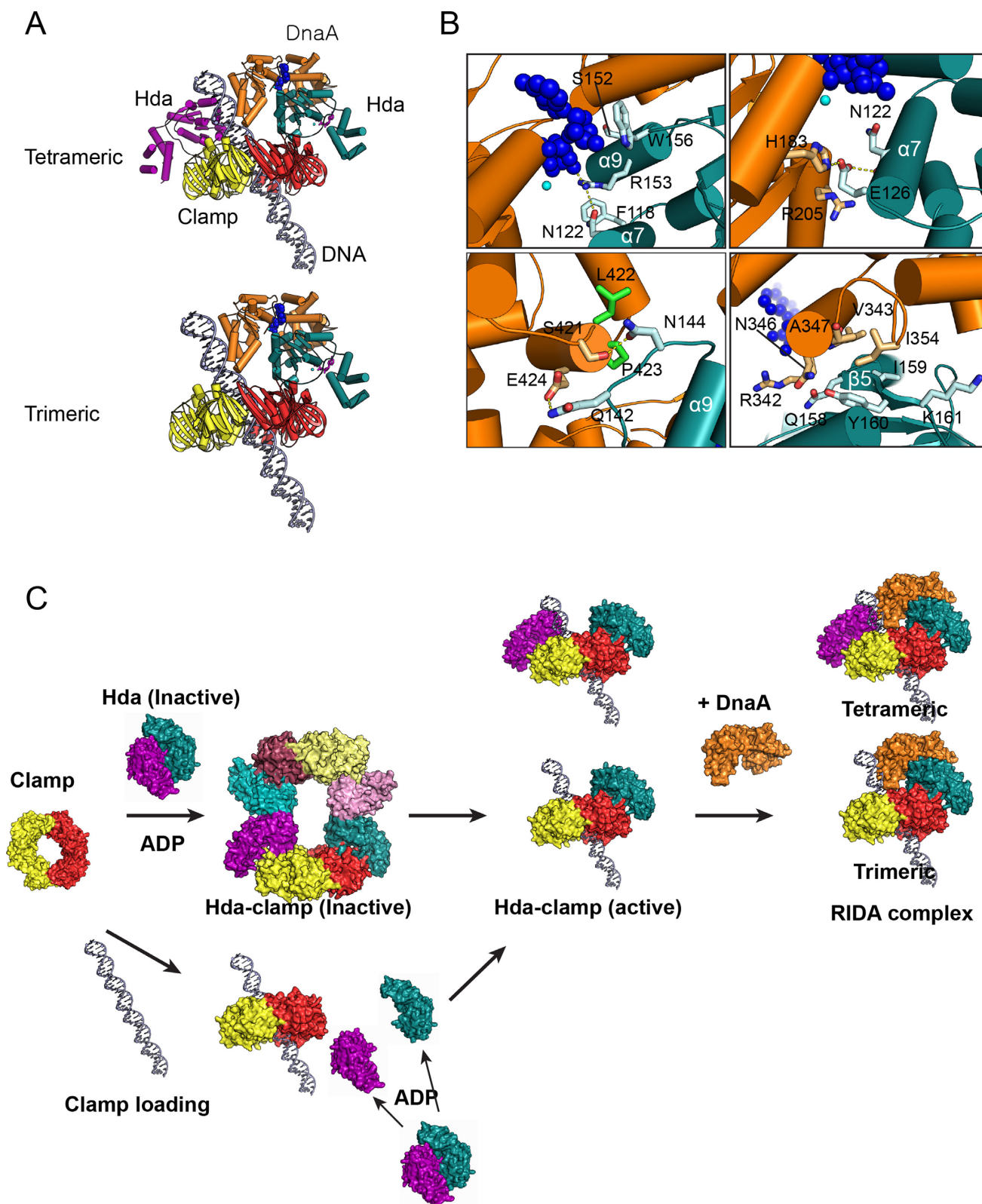). Higher levels (120 ng; data not shown) were unable to compensate for its defect in DNA binding. In addition, this mutant was assayed for its ability to stimulate the hydrolysis of ATP bound to DnaA (44). We found that the $\beta^{\Delta\text{loop}}$ mutant was defective in stimulating ATP hydrolysis. Comparing these results with those of Figure 6D and E that characterize the behavior of other mutants under essentially identical assay conditions, the results obtained with the $\beta^{\Delta\text{loop}}$ mutant demonstrate the requirement for DNA binding by the β clamp in the respective assays.

DISCUSSION

RIDA is one of the major mechanisms in bacteria to regulate the replication initiation, which is essential to maintain genomic stability (10,44–45). The Hda–β clamp complex loaded onto DNA plays a central role in RIDA by directly interacting with ATP-bound DnaA to stimulate its intrinsic DNA-dependent ATPase activity (10,19,30). In the present work, we determined the crystal and solution structure of the *E. coli* Hda–β clamp complex. A key feature of the complex is that it contains four Hda molecules sandwiched between two β clamps (Figure 1B–D). Each Hda makes two distinct contacts with the β clamp, with two Hda–β clamp tetramers associating through two tail-to-tail Hda homodimeric interfaces. Importantly, Hda homodimerization blocks access of the arginine finger of Hda (Arg153) to the γ-phosphate of ATP bound to DnaA, which is critical for ATP hydrolysis (Figure 2C). Thus, the octameric complex must disassemble to permit interaction of the arginine finger with DnaA.

On the basis of the X-ray structures of *Sa*Hda and *Aa*DnaA and biochemical analyses, others have suggested a model to describe how Hda functions in RIDA (13,15,21–22). In this model, a portion of the AAA+ domain of Hda comprising S127 to F140 that bears the sensor I residue (Arg137) is involved in the interaction with domains III and IV of of DnaA (13,15). Biochemically, this interaction requires the β clamp bound to both Hda and to DNA that has at least 40 bp of flanking DNA for the functional association between Hda and DnaA (9).

Based on our structure of the Hda–β clamp complex, we hypothesize that DnaA interacts with a complex containing either one Hda molecule and two clamps (trimer) or two Hda molecules and two β clamps (tetramer). We built models of the Hda–DnaA–β clamp–DNA complex by aligning the *Ec*Hda structure in the trimer or tetramer onto the ATP-exposed end of the tetrameric *Ec*DnaA that was generated from SWISS-MODEL using the *Aa*DnaA–ATP structure (Figure 7A and Supplementary Figure S7). Our models are similar to the heterodimer model of the *Sa*Hda–*Aa*DnaA complex in that they display contacts between the α7 and α9 helices of *Ec*Hda, which contains Box VI and VII motifs, and DnaA (15,21). In addition, *Ec*Hda's arginine finger interacts with the γ phosphate of ATP bound to DnaA (Figure 7B, upper left). Several Hda residues (F118, N122, S152 and R153) are also near the nucleotide-binding site of DnaA (Figure 7B, upper left and upper right). Of these, mutations of F118 and N122 (Box VI) affected RIDA activity (13), consistent with our model that they interact directly with DnaA.

Figure 7. Structural basis for RIDA. (**A**) Models of the complex containing the β clamp, Hda and DnaA bound to DNA. The model was built by aligning Hda (from the tetrameric or trimeric Hda–clamp complex) onto the DnaA dimer (generated from SWISS-MODEL). The chains of the *Ec*Hda–β clamp tetramer are represented by the same colors as in the octameric complex of Figure 1B; *Ec*DnaA is colored in orange. (**B**) The panels display the close-up views of the interfaces between *Ec*DnaA and *Ec*Hda. (**C**) RIDA activation model. Dimeric Hda forms a complex with the β clamp to form an inactive octamer. In the clamp loading process, the octameric complex dissociates and assembles on DNA as a trimeric or tetrameric complex. One possible mechanism involves one Hda molecule remaining bound to a protomer of the β clamp, which is loaded onto the DNA to form the trimer (not shown). Alternatively, Hda monomers bind to the β clamp already loaded on DNA to form a trimeric or tetrameric complex. To bind ATP-DnaA and to stimulate ATP hydrolysis, part of Hda may be released from the loop (residues 148–154) at interface 2.

Of interest, W156 is located at the interface between Hda and DnaA and makes contact with ADP. As we and others showed that an alanine substitute for Trp156 causes decreased RIDA activity (Figure 6D and E), but the substitution does not affect the affinity of Hda for ADP (13), we suggest that the W156A substitution impairs the ability of Hda to interact with DnaA. The regions that contain the end of the helix α7, loop α8–α9, and strand β5 of Hda are in close proximity with DnaA (Figure 7B). Residue E126 at the end of the helix α7 may form an ion pair with R205 of DnaA, and is also near H183 of DnaA (Figure 7B, upper right). In loop α8–α9 of Hda, Q142 and N144 are appropriately placed for hydrogen bonding with E424 and S421 in domain IV of DnaA, respectively, and very near L422 and P423 of DnaA, consistent with a model proposed by others (15, Figure 7B, lower left). The hydrophobic patch comprised of Q158, I159, Y160 and K161 in the β5 strand of Hda is well aligned with R342, V343, N346, A347 and I354 of domain IIIb of DnaA (Figure 7B, lower right). We propose that these residues stabilize the Hda–DnaA heterodimeric complex.

Published findings establish that Hda function requires the formation of interface 1 where the clamp binding motif of Hda interacts with the cleft of the β clamp (19,39). Biochemical and genetic analyses presented in this report demonstrate the importance of interfaces 2 and 3 that are critical for octamerization (Supplementary Table S5). As evidence, we found that substitution of residues comprising interface 2 of Hda failed to dissociate the complex, but instead altered its oligomeric state (Figure 1A and Supplementary Table S4). One or more substitutions may distort the interface such that the mutated surface or another segment(s) interacts with other parts of Hda and/or the β clamp. Of interest, the Hda[hook] mutant (K81S, W84S, F85S) targeting this interface actually stimulated RIDA activity. We suggest that one or more substitutions interfere with the formation interface 2 to predispose the interaction of Hda with ATP-DnaA.

By contrast, studies of a mutant clamp (β[Δloop]) lacking residues His148 to Tyr154 of the loop at interface 2 showed that a strain encoding the mutant clamp was inviable (30). As this loop is required for interaction with DNA during loading of the β clamp onto DNA (30,43), the failure of the mutant to support both DNA replication by DNA polymerase III and RIDA function is likely attributable to a loading defect. This loop also interacts with DNA polymerases II and IV, which is required for their processive DNA replication *in vitro* (30). These results underscore both the importance of non-cleft surfaces of the β clamp in managing the actions of its different partner proteins, and the dynamic nature of β clamp–partner interactions.

To stimulate the ATPase activity of ATP–DnaA, the arginine finger (Arg153) of Hda must interact with ATP–DnaA. In the octameric complex, however, the arginine finger is hidden by interface 3 formed between the two Hda protomers. Furthermore, Trp156, which is also important for RIDA, is buried within interface 3 (13). Hence, interface 3 must be disrupted to make the Hda–β clamp complex active. Of interest, the W156A substitution of Hda did not support octamer formation, but led to the formation of a tetrameric complex that presumably contains one β clamp

and two copies of Hda. Apparently, Trp156 plays a critical role in stabilizing interface 3 of the octamer. Despite the expectation that the mutant should be active in RIDA because its arginine finger should be exposed, it was impaired in RIDA activity. This result correlates with a previous study, which showed that the plasmid-borne mutation conferred dominant-negative lethality at 42°C after its introduction into an *hda*[+] strain (13). Thus, the W156A mutation impairs RIDA presumably because of the formation of an inactive complex with DnaA (13). Taken together, these findings suggest that the interaction between the Hda arginine finger and ATP bound to DnaA is controlled by two distinct sets of protein–protein interactions involving interface 3. Although the biological significance of the octameric Hda–β clamp complex requires further analysis, our results support the model that interface 3 plays a critical role in the interaction of Hda with ATP-DnaA. Moreover, while *Ec*Hda-ADP alone exists as a monomer, its interaction with the β clamp to form the octameric complex suggests that clamp-binding facilitates Hda homodimerization at interface 3. In support of this idea, Trp156 of *Ec*Hda, which is required for Hda homodimerization, exhibits a different conformation within the octamer than the equivalent residue (Trp164) of *Sa*Hda. This residue does not make contact with the β clamp (Figure 5A).

In the *in vitro* reconstituted RIDA assay, hydrolysis of DnaA-bound ATP is achieved by sequentially adding excess Hda to β clamp that is already loaded onto DNA (10,13,15,20,46). The cellular concentration of Hda is lower than either that of the β clamp or DnaA, and so Hda is believed to be recycled during RIDA (46–48). Furthermore, competition of Hda and the clamp loader for binding to the conserved clamp-binding cleft has been suggested to be a key factor in dissociating Hda from the β clamp (19). Thus, binding of the clamp loader to the β clamp may dissociate the octameric complex into free β clamp rings and Hda monomers. The subsequent binding of Hda to β clamp rings loaded onto DNA then forms the Hda–β clamp heterodimer that is active in RIDA (Figure 7C). In this case, the octamer may function to regulate the level of Hda made available for RIDA.

Collectively, our structural and functional analyses of the Hda–β clamp octameric complex reveal three interfaces. One canonical interface between the β clamp and Hda is essential for the stimulation of the ATPase activity of ATP-DnaA by Hda. In addition to this contact, two novel interfaces between the β clamp and Hda, and between Hda protomers may play negative regulatory roles that prevent activation of Hda in RIDA. Control of replication initiation is essential to maintain genomic stability in all living organisms. We suggest that the dynamic structure of the Hda–β clamp complex is important for fine-tuning Hda function during the regulation of replication initiation in bacteria.

ACCESSION NUMBER

The coordinates and structure factors of the *E. coli* Hda–β clamp crystal structure have been deposited in the Protein Data Bank under accession code 5x06.

REFERENCES

1. Skarstad,K. and Katayama,T. (2013) Regulating DNA replication in bacteria. *Cold Spring Harb. Perspect. Biol.*, **5**, a012922.
2. Riber,L., Frimodt-Møller,J., Charbon,G. and Løbner-Olesen,A. (2016) Multiple DNA binding proteins contribute to timing of chromosome replication in *E. coli. Front. Mol. Biosci.*, **3**, 29.
3. Duderstadt,K.E., Chuang,K. and Berger,J.M. (2011) DNA stretching by bacterial initiators promotes replication origin opening. *Nature*, **478**, 209–213.
4. Kaguni,J.M. (2006) DnaA: controlling the initiation of bacterial DNA replication and more. *Annu. Rev. Microbiol.*, **60**, 351–375.
5. Sutton,M.D., Carr,K.M., Vicente,M. and Kaguni,J.M., (1998) Escherichia coli DnaA protein. The N-terminal domain and loading of DnaB helicase at the E. coli chromosomal origin. *J. Biol. Chem.*, **273**, 34255–34262.
6. Makowska-Grzyska,M. and Kaguni,J.M. (2010) Primase directs the release of DnaC from DnaB. *Mol. Cell*, **37**, 90–101.
7. O'Donnell,M. (2006) Replisome architecture and dynamics in *Escherichia coli. J. Biol. Chem.*, **281**, 10653–10656.
8. Clarey,M.G., Erzberger,J.P., Grob,P., Leschziner,A.E., Berger,J.M., Nogales,E. and Botchan,M. (2006) Nucleotide-dependent conformational changes in the DnaA-like core of the origin recognition complex. *Nat. Struct. Mol. Biol.*, **13**, 684–690.
9. Su'etsugu,M., Takata,M., Kubota,T., Matsuda,Y. and Katayama,T. (2004) Molecular mechanism of DNA replication-coupled inactivation of the initiator protein in *Escherichia coli*: interaction of DnaA with the sliding clamp-loaded DNA and the sliding clamp-Hda complex. *Genes Cells*, **9**, 509–522.
10. Kato,J. and Katayama,T. (2001) Hda, a novel DnaA-related protein, regulates the replication cycle in *Escherichia coli. EMBO J.*, **20**, 4253–4562.
11. Leonard,A.C. and Grimwade,J.E. (2010) Regulating DnaA complex assembly: it is time to fill the gaps. *Curr. Opin. Microbiol.*, **13**, 766–772.
12. Fujimitsu,K., Su'etsugu,M., Yamaguchi,Y., Mazda,K., Fu,N., Kawakami,H. and Katayama,T. (2008) Modes of overinitiation, *dnaA* gene expression, and inhibition of cell division in a novel cold-sensitive *hda* mutant of *Escherichia coli. J. Bacteriol.*, **190**, 5368–5381.
13. Nakamura,K. and Katayama,T. (2010) Novel essential residues of Hda for interaction with DnaA in the regulatory inactivation of DnaA: unique roles for Hda AAA box VI and VII motifs. *Mol. Microbiol.*, **76**, 301–317.
14. Su'etsugu,M., Harada,Y., Keyamura,K., Matsunaga,C., Kasho,K., Abe,Y., Ueda,T. and Katayama,T. (2013) The DnaA N-terminal domain interacts with Hda to facilitate replicase clamp-mediated inactivation of DnaA. *Environ. Microbiol.*, **15**, 3183–3195.
15. Keyamura,K. and Katayama,T. (2011) DnaA protein DNA-binding domain binds to Hda protein to promote inter-AAA+ domain interaction involved in regulatory inactivation of DnaA. *J. Biol. Chem.*, **286**, 29336–29346.
16. Simmons,L.A., Breier,A.M., Cozzarelli,N.R. and Kaguni,J.M. (2004) Hyperinitiation of DNA replication in *Escherichia coli* leads to replication fork collapse and inviability. *Mol. Microbiol.*, **51**, 349–358.
17. Banack,T., Clauson,N., Ogbaa,N., Villa,J., Oliver,D. and Firshein,W. (2005) Overexpression of the Hda DnaA-related protein in *Escherichia coli* inhibits multiplication, affects membrane permeability, and induces the SOS response. *J. Bacteriol.*, **187**, 8507–8510.
18. Baxter,J.C. and Sutton,M.D. (2012) Evidence for roles of the *Escherichia coli* Hda protein beyond regulatory inactivation of DnaA. *Mol. Microbiol.*, **85**, 648–668.
19. Su'etsugu,M., Shimuta,T.R., Ishida,T., Kawakami,H. and Katayama,T. (2005) Protein associations in DnaA-ATP hydrolysis mediated by the Hda-replicase clamp complex. *J. Biol. Chem.*, **280**, 6528–6536.
20. Su'etsugu,M., Nakamura,K., Keyamura,K., Kudo,Y. and Katayama,T. (2008) Hda monomerization by ADP binding promotes replicase clamp-mediated DnaA-ATP hydrolysis. *J. Biol. Chem.*, **283**, 36118–36131.
21. Xu,Q., McMullan,D., Abdubek,P., Astakhova,T., Cariton,D., Chen,C., Chiu,H.J., Clayton,T., Das,D., Deller,M.C. *et al.* (2009) A structural basis for the regulatory inactivation of DnaA. *J. Mol. Biol.*, **385**, 368–380.
22. Kawakami,H., Su'etsugu,M. and Katayama,T. (2006) An isolated Hda-clamp complex is functional in the regulatory inactivation of DnaA and DNA replication. *J. Struct. Biol.*, **156**, 220–229.
23. Otwinowski,Z. and Minor,W. (1997) Processing of X-ray diffraction data collected in oscillation mode. *Methods Enzymol.*, **276**, 307–326.
24. Adams,P.D., Afonine,P.V., Bunkóczi,G., Chen,V.B., Davis,I.W., Echols,N., Headd,J.J., Hung,L.W., Kapral,G.J., Grosse-Kunstleve,R.W. *et al.* (2010) PHENIX: a comprehensive Python-based system for macromolecular structure solution. *Acta. Crystallogr. D Biol. Crystallogr.*, **66**, 213–221.
25. Emsley,P. and Cowtan,K. (2004) Coot: model-building tools for molecular graphics. *Acta. Crystallogr. D Biol. Crystallogr.*, **60**, 2126–2132.
26. Svergun,D.I., Barberato,C. and Koch,M.H.J. (1995) CRYSOL—a program to evaluate X-ray solution scattering of biological macromolecules from atomic coordinates. *J. Appl. Cryst.*, **28**, 768–773.
27. Petoukhov,M.V. and Svergun,D.I. (2015) Ambiguity assessment of small-angle scattering curves from monodisperse systems. *Acta Crystallogr. D Biol. Crystallogr.*, **71**, 1051–1058.
28. Riber,L. and Lobner-Olesen,A. (2005) Coordinated replication and sequestration of *oriC* and *dnaA* are required for maintaining controlled once-per-cell-cycle initiation in *Escherichia coli. J. Bacteriol.*, **187**, 5605–5613.
29. Datsenko,K.A. and Wanner,B.L. (2000) One-step inactivation of chromosomal genes in *Escherichia coli K-12* using PCR products. *Proc. Natl. Acad. Sci. U.S.A.*, **97**, 6640–6645.
30. Heltzel,J.M., Scouten Ponticelli,S.K., Sanders,L.H., Duzen,J.M., Cody,V., Pace,J., Snell,E.H. and Sutton,M.D. (2009) Sliding clamp-DNA interactions are required for viability and contribute to DNA polymerase management in *Escherichia coli. J. Mol. Biol.*, **387**, 74–91.
31. Ferullo,D.J. and Lovett,S.T. (2008) The stringent response and cell cycle arrest in *Escherichia coli. PLoS Genet.*, **4**, e1000300
32. Bradford,M.M. (1976) A rapid and sensitive method for the quantitation of microgram quantities of protein utilizing the principle of protein-dye binding. *Anal. Biochem.*, **72**, 248–254.
33. Marszalek,J. and Kaguni,J.M. (1992) Defective replication activity of a dominant-lethal dnaB gene product from *Escherichia coli. J. Biol. Chem.*, **267**, 19334–19340.
34. Johanson,K.O., Haynes,T.E. and McHenry,C.S. (1986) Chemical characterization and purification of the beta subunit of the DNA polymerase III holoenzyme from an overproducing strain. *J. Biol. Chem.*, **261**, 11460–11465.

35. Chodavarapu,S., Felczak,M.M., Simmons,L.A., Murillo,A. and Kaguni,J.M. (2013) Mutant DnaAs of *Escherichia coli* that are refractory to negative control. *Nucleic Acids Res.*, **41**, 10254–10267.

36. Bunting,K.A., Roe,S.M. and Pearl,L.H. (2003) Structural basis for recruitment of translesion DNA polymerase Pol IV/DinB to the beta-clamp. *EMBO J.*, **22**, 5883–5892.

37. Erzberger,J.P., Pirruccello,M.M. and Berger,J.M. (2002) The structure of bacterial DnaA: implications for general mechanisms underlying DNA replication initiation. *EMBO J.*, **21**, 4763–4773.

38. Erzberger,J.P., Mott,M.L. and Berger,J.M. (2006) Structural basis for ATP-dependent DnaA assembly and replication-origin remodeling. *Nat. Struct. Mol. Biol.*, **13**, 676–683.

39. Kurz,M., Dalrymple,B., Wijffels,G. and Kongsuwan,K. (2004) Interaction of the sliding clamp beta-subunit and Hda, a DnaA-related protein. *J. Bacteriol.*, **186**, 3508–3515.

40. Gon,S., Camara,J.E., Klungsøyr,H.K., Crooke,E., Skarstad,K. and Beckwith,J. (2006) A novel regulatory mechanism couples deoxyribonucleotide synthesis and DNA replication in *E. coli*. *EMBO J.*, **25**, 1137–1147.

41. Rosenkranz,H.Z., Winshell,E.B., Mednis,A., Carr,H.S. and Ellner,C.J. (1967) Studies with hydroxyurea. VII. Hydroxyurea and the synthesis of functional proteins. *J. Bacteriol.*, **94**, 1025–1033.

42. Sinha,N.K. and Snustad,D.P. (1972) Mechanism of inhibition of deoxyribonucleic acid synthesis in *Escherichia coli* by hydroxyurea. *J. Bacteriol.*, **112**, 1321–1324.

43. Georgescu,R.E., Kim,S.S., Yurieva,O., Kuriyan,J., Kong,X.P. and O'Donnell,M. (2008) Structure of a sliding clamp on DNA. *Cell*, **132**, 43–54.

44. Song,M.S. and McHenry,C.S. (2001) Carboxyl-terminal domain III of the delta' subunit of DNA polymerase III holoenzyme binds DnaX and supports cooperative DnaX complex assembly. *J. Biol. Chem.*, **276**, 48709–48715.

45. Camara,J.E., Breier,A.M., Brendler,T., Austin,S., Cozzarelli,N.R. and Crooke,E. (2005) Hda inactivation of DnaA is the predominant mechanism preventing hyperinitiation of *Escherichia coli* DNA replication. *EMBO Rep.*, **6**, 736–741.

46. Katayama,T., Kubota,T., Kurokawa,K., Crooke,E. and Sekimizu,K. (1998) The initiator function of DnaA protein is negatively regulated by the sliding clamp of the *E.coli* chromosomal replicase. *Cell*, **94**, 61–71.

47. Sekimizu,K., Yung,B.Y. and Kornberg,A. (1988) The dnaA protein of *Escherichia coli*. Abundance, improved purification, and membrane binding. *J. Biol. Chem.*, **263**, 7136–7140.

48. Chiaramello,A.E. and Zyskind,J.W. (1989) Expression of *Escherichia coli dnaA* and *mioC* genes as a function of growth rate. *J. Bacteriol.*, **171**, 4272–4280.